

RAP: KV-Cache Compression via RoPE-Aligned Pruning

Jihao Xin¹ Tian Lvu¹ David Keyes¹ Hatem Ltaief¹ Marco Canini¹

Abstract

Long-context inference in large language models is increasingly bottlenecked by the memory and compute cost of the KV-Cache. Low-rank factorization compresses KV projections by writing $\mathbf{W} \approx \mathbf{AB}$, where \mathbf{A} produces latent KV states and \mathbf{B} can be absorbed into downstream weights. In modern RoPE-based LLMs, this absorption fails: RoPE forces latent KV states to be reconstructed to full dimension, reintroducing substantial memory and compute overhead. We propose *RoPE-Aligned Pruning (RAP)*, which prunes entire RoPE-aligned column pairs to preserve RoPE’s 2×2 rotation structure, restore \mathbf{B} absorption, and eliminate reconstruction. Our evaluation on LLaMA-3-8B and Mistral-7B shows that RAP enables joint reduction of KV-Cache, attention parameters, and FLOPs by 20%–30%, all at once, while maintaining strong accuracy. Notably, RAP reduces attention latency to 83% (prefill) and 77% (decode) of baseline.

1. Introduction

Large Language Models (LLMs) (Achiam et al., 2023; Touvron et al., 2023; Bai et al., 2023; Liu et al., 2024a) have achieved remarkable progress through scaling model size and context length (Gholami et al., 2024). However, long-context inference remains bottlenecked by the ever-expanding key-value (KV) cache. For instance, a 30B-parameter model at 100K context consumes 22.8 GB solely for the KV-Cache (Fu, 2024), motivating effective compression for deployment on commodity hardware.

Prior work includes *direct KV-Cache compression* (e.g., quantization, eviction) and *weight decomposition* (Section 2.2). We build on the latter—reducing \mathbf{W} ’s dimensionality so that KV states are low-dimensional. The standard approach is SVD-based low-rank factorization (Wang et al., 2025b), which factorizes \mathbf{W} as $\mathbf{W} \approx \mathbf{AB}$, retaining

a fraction of the dimension:

$$\begin{aligned} \mathbf{XW} &\approx \mathbf{XU}_{\hat{D}D'} \boldsymbol{\Sigma}_{D'D'} \mathbf{V}_{D'D'}^\top \\ &= \mathbf{X} \underbrace{\left(\mathbf{U}_{\hat{D}D'} \boldsymbol{\Sigma}_{D'D'}^{1/2} \right)}_{\mathbf{A}} \underbrace{\left(\boldsymbol{\Sigma}_{D'D'}^{1/2} \mathbf{V}_{D'D'}^\top \right)}_{\mathbf{B}} \end{aligned} \quad (1)$$

$\mathbf{X} \in \mathbb{R}^{1 \times \hat{D}}$ is the input embedding, $\mathbf{W} \in \mathbb{R}^{\hat{D} \times D}$ is the projection weight, D is the per-head dimension, \hat{D} is the model dimension, and D' is the per-head retained dimension. We define ρ as the KV-Cache compression ratio, and r as the retained ratio, i.e., $\rho = 1 - r$. Instead of caching the original $\mathbf{K} = \mathbf{XW}_k$ and $\mathbf{V} = \mathbf{XW}_v$, storing only the latent representation \mathbf{XA} can reduce cache size by ρ , but requires reconstructing $\mathbf{XA} \cdot \mathbf{B}$ at every decoding step (Figure 1). To address this, PaLU (Chang et al., 2025) attempts to absorb \mathbf{B}_k into \mathbf{W}_q and \mathbf{B}_v into \mathbf{W}_o to eliminate the reconstruction. However, most modern LLMs apply RoPE after the Q/K projections to improve extrapolation, making such absorption impractical due to the lack of **RoPE-commutativity**:

Definition 1.1. A factorization $\mathbf{W} \approx \mathbf{AB}$ satisfies RoPE-commutativity if $\text{RoPE}(\mathbf{XA})\mathbf{B} = \text{RoPE}(\mathbf{XAB})$.

Alternatively, RAP employs structured pruning to reduce the weight dimension by eliminating entire RoPE-aligned column pairs. Similar to factorization, RAP also constructs \mathbf{A} and \mathbf{B} but with guaranteed RoPE-commutativity by pruning at the pair granularity, preserving the rotational structure. Consequently, \mathbf{B} can be absorbed into downstream weights, completely eliminating the reconstruction overhead.

Contributions. (i) We identify **RoPE-commutativity** as the missing condition for *weight decomposition*. (ii) RAP leverages structured pruning specifically for KV-Cache compression under RoPE constraints. (iii) We provide a drop-in pipeline (Fisher scores, adaptive budgets, non-contiguous RoPE kernel) that makes these gains practical. (iv) RAP is the only overhead-free method we evaluated that jointly reduces KV-Cache, parameters, and FLOPs.

2. Background

2.1. Transformers and Attention Mechanism

Modern LLMs are built upon *decoder-only transformers* with multi-head attention (MHA) modules, trained with an

¹KAUST, Saudi Arabia. Correspondence to: Jihao Xin <jihao.xin@kaust.edu.sa>.

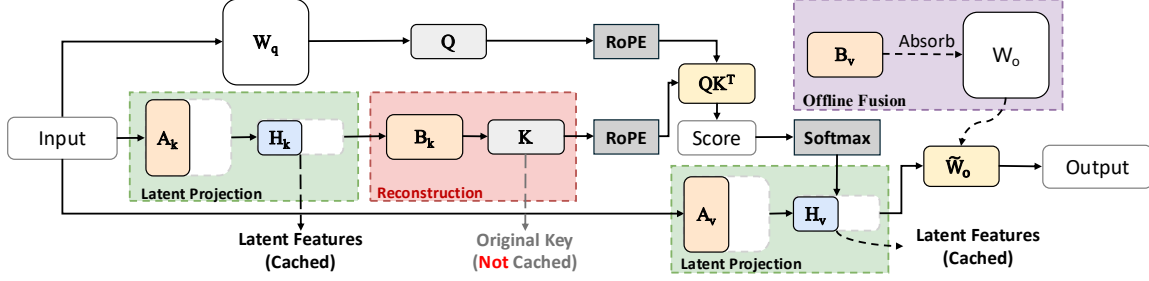


Figure 1. SVD-based KV-Cache compression requires full-dimensional reconstruction at runtime.

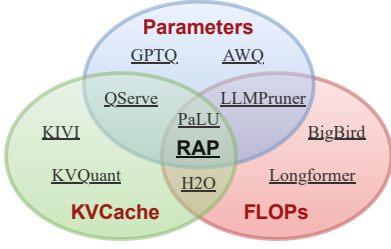


Figure 2. Optimizations of KV-Cache/FLOPs/Parameters.

autoregressive objective (Vaswani et al., 2017). During the decoding phase, the model processes one token at a time. Given the input embedding $\mathbf{X}_t \in \mathbb{R}^{1 \times \hat{D}}$ at step t , each attention head projects it into queries, keys, and values:

$$\mathbf{Q}_t = \mathbf{X}_t \mathbf{W}_q, \quad \mathbf{K}_t = \mathbf{X}_t \mathbf{W}_k, \quad \mathbf{V}_t = \mathbf{X}_t \mathbf{W}_v, \quad (2)$$

where $\mathbf{W}_q, \mathbf{W}_k, \mathbf{W}_v \in \mathbb{R}^{\hat{D} \times D}$, and $D = \hat{D}/H$ is the per-head dimension, H is the number of attention heads. The newly computed \mathbf{K}_t and \mathbf{V}_t are appended to the previous steps' \mathbf{K} and \mathbf{V} , forming the **KV-Cache**. The attention output of each head each step is given by:

$$\text{AttnOut} = \text{softmax}\left(\frac{\mathbf{Q}\mathbf{K}^\top}{\sqrt{D}}\right) \mathbf{V}\mathbf{W}_o, \quad [1] \quad (3)$$

where $\mathbf{W}_o \in \mathbb{R}^{D \times \hat{D}}$ is the output projection. This caching mechanism avoids recomputing \mathbf{K} and \mathbf{V} at each step, reducing the time complexity of projection from quadratic to linear with sequence length, but the accumulated KV-Cache grows linearly with sequence length, posing a major memory bottleneck for long-context inference.

2.2. KV-Cache Compression and Model Pruning

Traditional **Direct KV-Cache Compression** primarily falls into three categories: *KV-Cache quantization* (Liu et al., 2024b; Hooper et al., 2024) stores KV activations in lower precision; *token eviction* (Li et al., 2024; Zhang et al., 2023) removes less important tokens to shorten the effective context; *KV Pruning* (Lv et al., 2025) prunes KV-Cache channels without modifying the model weights. Instead of direct

^[1]This formulation omits bias terms, causal masking, positional embeddings, and subscripts for time steps and heads for simplicity.

KV-Cache compression, **Weight Decomposition** (Chang et al., 2025) factorizes the projection weights into 2 smaller matrices and absorbs the second matrix into downstream weights, which improves KV-Cache compression while reducing parameters and FLOPs. However, it fails in modern LLMs due to RoPE incompatibility (Section 3).

Orthogonally, **Model Pruning** is widely adopted to reduce model parameters. However, existing pruning methods focus on parameter reduction rather than KV-Cache compression; that is, no approach has been proposed to work around RoPE. In practice, standard approaches either avoid pruning attention weights altogether or remove the entire head (Ma et al., 2023), both of which are suboptimal. Inspired by it, RAP leverages structured pruning while enforcing RoPE-commutativity constraint to achieve simultaneous KV-Cache, parameters, and FLOPs reductions.

Moreover, parameter quantization (Frantar et al., 2022; Lin et al., 2024; 2025) and efficient-attention variants (Beltagy et al., 2020; Zaheer et al., 2020) also provide complementary savings (they do not compress KV-Cache, so we did not evaluate them). Figure 2 summarizes these directions.

Direct KV-Cache Compression is orthogonal to our approach and can be used as combined strategies (verified in PaLU and our evaluation). Existing model pruning is not designed for KV-Cache compression. Therefore, we compare primarily against factorization baselines, which target the same goal of reducing KV-Cache dimensionality.

3. Motivation: RoPE Incompatibility

Most modern LLMs use **RoPE** to encode positional information by applying rotations in paired dimensions (Table 1). Given a token position i , RoPE is formulated as:

$$\text{RoPE}\left(\begin{bmatrix} k_{i,j} \\ k_{i,j'} \end{bmatrix}\right) = \mathbf{R}(i, \theta_j) \begin{bmatrix} k_{i,j} \\ k_{i,j'} \end{bmatrix}, \quad (4)$$

where $\mathbf{R}(i, \theta_j) = \begin{bmatrix} \cos(i\theta_j) & -\sin(i\theta_j) \\ \sin(i\theta_j) & \cos(i\theta_j) \end{bmatrix}$, $\theta_j = \theta_{\text{base}}^{-2j/D}$, θ_{base} is a constant. Taking \mathbf{K} as an example, it is grouped into *RoPE pairs* (j, j') , where the pairing strategy varies across models (e.g., $j = 2x - 1, j' = 2x$ or $j = x, j' =$

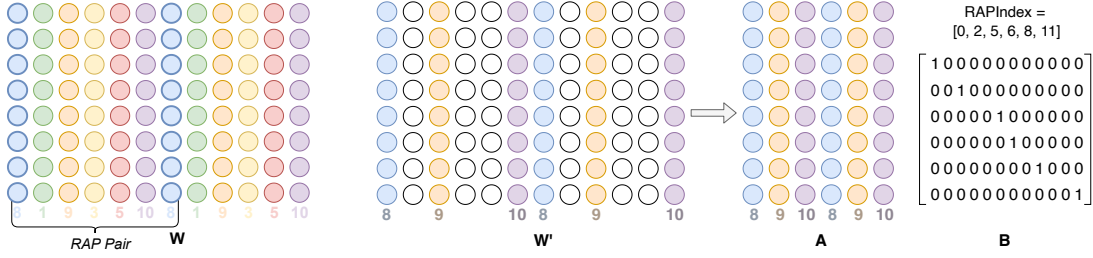


Figure 3. RAP Example: Weight matrix \mathbf{W} with 12 columns is grouped into 6 RoPE pairs, then pruned 50% based on the RoPE scores.

Table 1. Major open-source LLMs use RoPE (Zhipu AI, 2026; DeepSeek, 2025; Mistral, 2025; Qwen, 2025; OpenAI, 2025; Meta AI, 2025).

MODEL NAME	RELEASE DATE	POSITIONAL EMBEDDING
GLM-4.7	JAN 2026	RoPE
DEEPMSEEK-V3.2	DEC 2025	RoPE
MISTRAL-3.2	DEC 2025	RoPE
QWEN-3	SEP 2025	RoPE
GPT-OSS	AUG 2025	RoPE
LLAMA-4	APR 2025	RoPE

Table 2. Resource requirements of computing KV-Cache for one attention head. D =per-head dimension, H =total heads and HD =model dimension, S =sequence length.

Method	KV-Cache	Parameters	FLOPs
Baseline (\mathcal{B})	$2SD$	$2HD^2$	$4SHD^2$
SVD	$r\mathcal{B}$	$(r + \frac{r}{H})\mathcal{B}$	$(r + \frac{r}{H})\mathcal{B}$
PaLU	$r\mathcal{B}$	$(r + \frac{r}{2H})\mathcal{B}$	$(r + \frac{r}{2H})\mathcal{B}$
RAP	$r\mathcal{B}$	$r\mathcal{B}$	$r\mathcal{B}$

$x + D/2$ for $x \in [1, D/2]$.

Dimension-reduction methods promise to reduce both memory and computation by decomposing the projection weights. For example, SVD factorization $\mathbf{W}_k \approx \mathbf{A}_k \mathbf{B}_k$ from Eq. (1), without positional embeddings, \mathbf{B}_k can be absorbed into the query projection ($\widetilde{\mathbf{W}}_q = \mathbf{W}_q \mathbf{B}_k^\top \in \mathbb{R}^{\hat{D} \times rD}$). However, modern LLMs apply RoPE *after* Q/K projections (Figure 1). Since SVD-based methods break RoPE’s pairing semantics, traditional factorizations **do not commute with RoPE** and thus block absorption: $\text{RoPE}(\mathbf{XA}_k \mathbf{B}_k) \neq \text{RoPE}(\mathbf{XA}_k) \mathbf{B}_k$. Consequently, reconstructing \mathbf{K} to full dimension incurs significant memory and computational overhead. RAP resolves this incompatibility by constructing the low-dimensional \mathbf{A}_k and \mathbf{B}_k through structured pruning with RoPE-commutativity constraint. Table 2 compares KV projection (K/V) resource cost of each method (Derivation in Appendix C). In the worst-case like Single-Head Attention, SVD achieves reductions in parameters and FLOPs only when $\rho > 50\%$, and PaLU only when $\rho > 33\%$. To the best of our knowledge, RAP is the only method that guarantees linear reductions in KV-Cache, parameters, and

FLOPs simultaneously.

4. RAP: RoPE-Aligned Pruning

RAP constructs \mathbf{A} and \mathbf{B} so that $\mathbf{W} \approx \mathbf{AB}$ to satisfy RoPE-commutativity (Definition 1.1), i.e.,

$$\text{RoPE}(\mathbf{XW}) \approx \text{RoPE}(\mathbf{XAB}) = \text{RoPE}(\mathbf{XA})\mathbf{B} \quad (5)$$

To clarify, for compressed matrices (e.g., \mathbf{XA}), $\text{RoPE}(\cdot)$ denotes an *index-aware* RoPE that uses the original dimension indices of the retained RoPE pairs. This commutativity enables absorbing \mathbf{B} into downstream layers, eliminating reconstruction FLOPs while reducing both parameters and KV-Cache. To preserve commutativity, the factorization must respect RoPE’s 2×2 rotation blocks.

Structured pruning presents itself as a promising alternative (Ma et al., 2023) in reducing parameters. However, pruning arbitrary columns still breaks these rotation blocks and thus fails to preserve commutativity. Therefore, RAP applies the commutativity constraint with a minimal block-preserving transformation: pruning whole *RoPE pairs*, preserving rotation semantics and ensuring Eq. (5) holds.

We summarize the RAP pipeline in Algorithm 1, and detail each component in the following subsections.

4.1. Step 1: RoPE Pair Scoring

Given an LLM, we first identify all RoPE-sensitive attention heads and gather their K V projection weights as \mathcal{W} (Algorithm 1, line 1). For each $\mathbf{W} \in \mathcal{W}$ with $\mathbf{W} \in \mathbb{R}^{\hat{D} \times D}$, we group its columns into RoPE pairs according to the target model’s pairing strategy (Algorithm 1, line 2). Each pair (j, j') corresponds to two dimensions that RoPE rotates together via a single 2×2 block, as discussed in Section 3. We denote the set of all such pairs as \mathcal{P} , with $|\mathcal{P}| = D/2$. Figure 3 illustrates this grouping: a weight matrix \mathbf{W} with 12 columns is partitioned into 6 RoPE pairs (denoted by different colors). By organizing columns in this manner, RAP ensures that any subsequent pruning operation removes or retains complete rotation blocks atomically, never breaking the paired structure required by Eq. (5).

Algorithm 1 RoPE-Aligned Pruning (RAP)

Require: Model \mathcal{M} , calibration dataset \mathcal{D} , compression ratio ρ
Ensure: Pruned model $\widetilde{\mathcal{M}}$ with low-dimensional weights

- 1: Identify all RoPE-sensitive projection weights \mathcal{W}
- 2: For each $\mathbf{W} \in \mathcal{W}$, partition columns into RoPE pairs \mathcal{P} and compute importance scores (Fisher information) σ_p on \mathcal{D}
- 3: Allocate compression budgets using Alg. 2 (per-layer ratios, with differentiated K/V allocation)
- 4: **for** each RoPE-sensitive projection $\mathbf{W} \in \mathcal{W}$ **do**
- 5: Determine budget m (number of pairs to retain) based on allocated compression ratio
- 6: Remove least significant RoPE pairs according to σ_p ; keep top m pairs to form pruned matrix \mathbf{A}
- 7: Construct binary expansion matrix \mathbf{B} that maps \mathbf{A} back to original dimensions (Eq. (8))
- 8: Absorb \mathbf{B} into downstream weights
- 9: **end for**
- 10: Apply knowledge distillation to pruned model with LoRA
- 11: Merge LoRA adapters into base weights for deployment

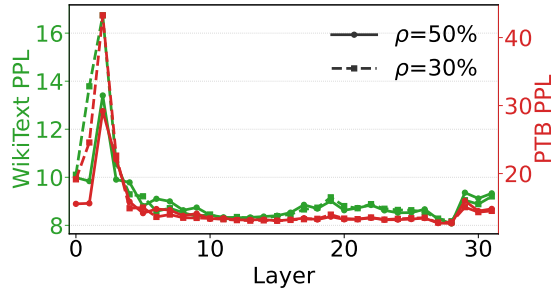


Figure 4. LLaMA PPL of pruning one layer at a time.

To quantify the importance of each RoPE pair, we adopt *Fisher information*, which approximates the Hessian (Frantar & Alistarh, 2023) by accumulating gradient statistics, offering a computationally efficient proxy for parameter importance:

$$\mathbf{F}(\mathbf{W}) = \mathbb{E}_{(x,y) \sim \mathcal{D}} \left[\left(\frac{\partial \mathcal{L}(x, y)}{\partial \mathbf{W}} \right)^2 \right], \quad (6)$$

where \mathcal{L} is the model loss and \mathcal{D} is a small calibration dataset (typically a few thousand tokens). For each RoPE pair $p = (j, j') \in \mathcal{P}$, we aggregate the Fisher scores over the two columns forming the pair, where $\mathbf{F}(\mathbf{W})_{:,i}$ denotes the Fisher information for column i of \mathbf{W} :

$$\sigma_p = \sum_{i \in \{j, j'\}} \sum_n \mathbf{F}(\mathbf{W})_{n,i}, \quad (7)$$

4.2. Step 2: Budget Allocation

Next, we allocate pruning budgets under a global compression ratio ρ (Algorithm 1, line 3). The most straightforward approach is uniform allocation, which applies the same ρ across all weights, ignoring sensitivity differences. Instead,

Algorithm 2 Adaptive Budget Allocation

Require: Weights \mathcal{W} (all layers, K and V), pair scores $\{\sigma_p\}$, compression ratio ρ
Ensure: Compression ratios $\{\rho_{\ell,i}\}$

- 1: Partition \mathcal{W} into groups (ℓ, i) , ℓ is layer index, i is group index
- 2: Compute number of groups: $N \leftarrow |\{(\ell, i)\}|$
- 3: Compute total score: $SC \leftarrow \sum \sigma_p$
- 4: **for** each group (ℓ, i) **do**
- 5: Aggregate pair scores: $\sigma_{\ell,i} \leftarrow \sum_{p \in \mathcal{P}_{\ell,i}} \sigma_p$
- 6: Assign raw ratio with normalization: $\tilde{\rho}_{\ell,i} \leftarrow \rho \cdot \frac{1 - \sigma_{\ell,i}/SC}{1 - 1/N}$
- 7: Clamp to a valid range: $\rho_{\ell,i} \leftarrow \text{clip}(\tilde{\rho}_{\ell,i}, 0, 1)$
- 8: **end for**
- 9: Project $\{\rho_{\ell,i}\}$ onto $[0, 1]$ with mean ρ
- 10: Uniformly distribute $\rho_{\ell,i}$ across all heads within each group

we employ *adaptive budget allocation* at three levels: **(1) Differentiated K and V.** Within a layer, we allocate different budgets for \mathbf{W}_k and \mathbf{W}_v based on their sensitivity. Our experiments show that \mathbf{V} is typically more sensitive than \mathbf{K} ; for example, with $\rho=30\%$ on LLaMA, the average retained rank fraction is 45% for \mathbf{K} but 96% for \mathbf{V} . **(2) Uniform across heads.** Within a layer, given a weight matrix \mathbf{W}_k or \mathbf{W}_v , we keep the same retained dimension across all heads to enable efficient batched General Matrix Multiply (GEMM) implementations. **(3) Adaptive across layers.** Layers exhibit pronounced sensitivity differences: Figure 4 shows pruning the front and back layers has a higher impact on perplexity (PPL) than the middle layers. We rank all weight groups across layers based on Fisher scores (e.g., 64 groups for a 32-layer model) and allocate less pruning budget to more sensitive groups. Algorithm 2 summarizes this procedure.

4.3. Step 3: RAP Construction

Given the selected RoPE pairs, we construct the approximation $\mathbf{W} \approx \mathbf{AB}$ and absorb \mathbf{B} into downstream weights (Algorithm 1, lines 5–8). First, the retained columns naturally form $\mathbf{A} \in \mathbb{R}^{\hat{D} \times 2m}$, where m is the number of retained pairs. Then, we introduce a binary expansion matrix $\mathbf{B} \in \mathbb{R}^{2m \times D}$ that maps \mathbf{A} back to the original positions:

$$B_{i,j} = \begin{cases} 1 & \text{if } \text{RAPIndex}[i] = j, \\ 0 & \text{otherwise,} \end{cases} \quad (8)$$

where $\text{RAPIndex}[i]$ gives the original column index of the i -th retained column (Figure 3). The key insight is that \mathbf{B} commutes with RoPE due to its pair-preserving structure. Therefore, the attention computation can be written as:

$$\mathbf{QK}^\top = \text{RoPE}(\mathbf{XW}_q \mathbf{B}_k^\top) \text{RoPE}(\mathbf{XA}_k)^\top, \quad (9)$$

We absorb \mathbf{B}_k^\top into the query projection by computing $\widetilde{\mathbf{W}}_q = \mathbf{W}_q \mathbf{B}_k^\top \in \mathbb{R}^{\hat{D} \times 2m}$, yielding:

$$\mathbf{QK}^\top = \text{RoPE}(\mathbf{X}\widetilde{\mathbf{W}}_q) \text{RoPE}(\mathbf{XA}_k)^\top. \quad (10)$$

Both query and key projections are now low-rank ($\hat{D} \times 2m$), and the cache stores only $\mathbf{K}_{\text{latent}} = \text{RoPE}(\mathbf{X}\mathbf{A}_k) \in \mathbb{R}^{S \times 2m}$, where S is the sequence length. This is the key advantage over SVD-based methods: the reconstruction matrix \mathbf{B} is absorbed, leaving the inference graph unchanged.

4.4. Step 4: Accuracy Recovery

Finally, we apply accuracy recovery after pruning (Algorithm 1, line 10). Structured pruning inevitably removes informative features, leading to accuracy degradation; we primarily employ Knowledge Distillation (KD) (Hinton et al., 2015) to align the compressed student with the original teacher for recovery (Ma et al., 2023; Frantar & Alistarh, 2023; Sun et al., 2024). To minimize training cost, we adopt Low-Rank Adopter (LoRA) (Hu et al., 2022), which keeps the base model frozen and trains only a small set of adapter parameters. LoRA augments a frozen weight matrix $\mathbf{W} \in \mathbb{R}^{d_{\text{in}} \times d_{\text{out}}}$ with trainable low-rank factors:

$$\mathbf{W}' = \mathbf{W} + \mathbf{L}_{\text{down}}\mathbf{L}_{\text{up}}, \quad (11)$$

where $\mathbf{L}_{\text{down}} \in \mathbb{R}^{d_{\text{in}} \times r_{\text{LoRA}}}$ and $\mathbf{L}_{\text{up}} \in \mathbb{R}^{r_{\text{LoRA}} \times d_{\text{out}}}$ with $r_{\text{LoRA}} \ll \min(d_{\text{in}}, d_{\text{out}})$. After KD, we merge the adapters back to the original weight, thus there is no runtime overhead (Algorithm 1, line 11).

In RAP, we apply KD to $\mathbf{W}_q, \mathbf{W}_k, \mathbf{W}_v, \mathbf{W}_o$ with LoRA rank $r_{\text{LoRA}}=8$, which takes only < 1% of model size. For calibration, we use the WikiText-2 dataset by default; other datasets such as C4 are also effective. We combine cross-entropy (CE) loss on ground-truth labels with Kullback-Leibler (KL) divergence between teacher and student logits:

$$\mathcal{L} = \mathcal{L}_{\text{CE}} + \mathcal{L}_{\text{KD}}, \quad (12)$$

where \mathcal{L}_{CE} is the CE loss and \mathcal{L}_{KD} is the KL divergence:

$$\mathcal{L}_{\text{KD}} = \mathbb{E}_{x \sim \mathcal{D}} [\text{KL}(P_{\text{teacher}}(\cdot | x) \| P_{\text{student}}(\cdot | x))], \quad (13)$$

where P_{teacher} and P_{student} denote the output probability distributions of the teacher and student models, and \mathcal{D} is the calibration dataset. The KD term is the primary mechanism that leverages teacher’s soft predictions to improve generalization after pruning, while the CE term provides additional task accuracy signal.

4.5. Practical Considerations

Compatibility with RoPE variants. As RoPE gains widespread adoption, specialized extensions such as YaRN (Peng et al., 2023) and Circle-RoPE (Wang et al., 2025a) have also been widely deployed. Although RAP is designed based on the mainstream RoPE implementation, it seamlessly supports these variants since they primarily modify scaling factors, frequency parameters, or pairing strategies while preserving the core rotation logic that RAP’s commutativity property relies on.

Hybrid low-dimensional compression. RAP addresses the RoPE incompatibility, while SVD-based factorization guarantees theoretically optimal approximation in Frobenius norm. To leverage the strengths of both methods, our default pipeline identifies where RoPE is applied and uses RAP for those components, while applying factorization to the remaining parts. In most modern LLMs, RoPE is applied only to \mathbf{Q} and \mathbf{K} projections, where we apply RAP to compress \mathbf{W}_k and use SVD to compress \mathbf{W}_v ; after absorption, \mathbf{W}_q and \mathbf{W}_o will be automatically compressed. For emerging architectural variants—such as LLaMA-4’s interpolated RoPE (iRoPE), which applies RoPE selectively to certain layers—we apply RAP only to those RoPE-augmented layers and use SVD for the remaining layers. This hybrid strategy guarantees correct handling of positional embeddings and maintains optimal accuracy in general.

Efficient non-contiguous RoPE kernel. In standard RoPE implementations, the cos / sin matrices are pre-computed once per forward pass and efficiently broadcast across heads and layers. After RAP, heads and layers retain different RoPE pairs, so applying RoPE requires per-head indexing of cos / sin. In PyTorch, such non-contiguous indexing often materializes new tensors, which incurs a small overhead. We show that this is a “fake overhead” due to PyTorch’s unnecessary memory copy. We solve it by writing a custom Triton kernel that applies RoPE to non-contiguous pairs using per-head offsets, directly reading the needed subsets of cos / sin during rotation without extra buffer allocation. Therefore, RAP introduces no overhead—the computation graph is unchanged from the baseline except the dimension reduction. Performance comparisons are in Section 6.

5. RoPE-Invariant Error Bounds

We provide theoretical analysis for RAP’s error bounds. Unlike SVD, RAP introduces no approximation error from basis rotation. Instead, its error arises solely from removing RoPE pairs. We show this error is bounded, RoPE-invariant, and minimized by the pair-scoring criterion.

Setup. We consider a single attention head and omit layer/head indices. Let $W_q, W_k \in \mathbb{R}^{\hat{D} \times D}$ be the query and key projections, and $X \in \mathbb{R}^{S \times \hat{D}}$ the token activations, where S is the sequence length and \hat{D} is the model dimension. RAP groups columns of W_k into RoPE pairs $\mathcal{P} = \{(j_1, j'_1), \dots, (j_{D/2}, j'_{D/2})\}$ and retains $\mathcal{S} \subset \mathcal{P}$ of size m . The pruned key projection is $A_k \in \mathbb{R}^{\hat{D} \times 2m}$, and the absorbed query projection is $\tilde{W}_q = W_q B_k^\top \in \mathbb{R}^{\hat{D} \times 2m}$ ((10)), ensuring dimensional consistency but not affecting the loss analysis below. Since RoPE applies orthogonal transformations that preserve Euclidean norms, removing entire RoPE pairs commutes with the transformation. This structure uniquely allows us to analyze pruning error as

additive contribution from independent pairs.

Theorem 5.1 (Loss induced by RoPE-aware pair pruning). *Let $\mathcal{L}(\cdot)$ denote the model’s training loss as a function of the key projection matrix, with all other parameters held fixed. Let A_k denote the pruned matrix obtained by RAP by removing RoPE pairs $\mathcal{P} \setminus \mathcal{S}$. Under a second-order Taylor approximation of \mathcal{L} around W_k , the pruning-induced loss satisfies*

$$\Delta\mathcal{L} \triangleq \mathcal{L}(A_k) - \mathcal{L}(W_k) \leq \frac{1}{2} \sum_{p \notin \mathcal{S}} \sigma_p, \quad (14)$$

where σ_p is the Fisher score defined in Eq. (7).

(Proof in Appendix B.)

Corollary 5.2 (Optimality of Fisher-based RoPE pair selection). *The pruning strategy \mathcal{S} that minimizes the loss upper bound in the above theorem is given by selecting the m pairs with the largest Fisher scores σ_p . Specifically, the problem $\min_{\mathcal{S}:|\mathcal{S}|=m} \sum_{p \notin \mathcal{S}} \sigma_p$ is solved by retaining the pairs with the highest importance scores.*

6. Experiments

6.1. Setup

Models and Datasets. We evaluate RAP on LLaMA (LLaMA-3-8B-Instruct) and Mistral (Mistral-7B-v0.3), comparing against no compression (Baseline), SVD-LLM (SVD), and PaLU. We use PPL as the primary quality metric, which aligns closely with zero-shot accuracy on commonsense tasks (lm-eval), and long-context performance on LongBench. We also demonstrate RAP’s orthogonality combined with quantization. For brevity, main-text figures primarily show LLaMA results; corresponding Mistral plots are provided in Appendix D.1.

Compression Settings. Throughout this paper, the compression ratio ρ specifically refers to the *KV-Cache compression ratio*. We test $\rho \in [10\%, 50\%]$. Fisher scores are estimated over a small calibration set ($N=32$ windows of length $L=2048$ from Wikitext-2-raw-v1); results are insensitive to calibration dataset. Factorization methods (SVD and PaLU) can operate at per-head or cross-head granularity. Per-head is the most efficient: same compression ratio yields fewest parameters and lowest reconstruction FLOPs. PaLU can only absorb \mathbf{B}_v into \mathbf{W}_o under per-head factorization. Table 3 shows ranges for the model size and FLOPs from per-head (optimal) to cross-head, which demonstrates per-head is the most efficient setting. Therefore, all reported curves use per-head by default. At inference, SVD reconstructs both K and V to full dimension (naive per-head truncated SVD on $\mathbf{W}_k/\mathbf{W}_v$; no RoPE absorption, no adaptive budget, no data whitening), which results in higher latency and poor accuracy. On top of SVD, PaLU applies

data whitening and absorbs \mathbf{B}_v into \mathbf{W}_o , and reconstructs only K. RAP absorbs \mathbf{B}_k into \mathbf{W}_q and \mathbf{B}_v into \mathbf{W}_o , eliminating all reconstruction overhead. Reproducibility details are provided in Appendix D.4.

Comparison Fairness of KD. We evaluate SVD/PaLU as post-training factorization baselines *without* KD (SVD is the optimal rank- r approximation in Frobenius norm (Eckart & Young, 1936)). Since pruning can induce distribution shift, we follow standard pruning practice (e.g., LLM-Pruner) and apply only a short, lightweight KD to RAP (LoRA $r_{\text{LoRA}}=8$, $\alpha=16$, dropout 0.05, < 1% parameters), using a combined CE+KD loss (temperature 2.0) on Wikitext-2 and merging LoRA adapters into base weights before evaluation; on LLaMA at $\rho=30\%$, KD converges quickly: PPL recovers from 28.86 (pruned) to 9.70 within one epoch (25 min) and reaches 8.82 within 2.9 hours. We also experimented with PaLU+KD (Appendix D.3), but observed only marginal, hyperparameter-sensitive gains; thus we omit it from the main comparisons.

Hardware and Software. We use one NVIDIA A100-80GB GPU with Python 3.10.18, PyTorch 2.4.0+cu121 (CUDA 12.1), and transformers 4.57.0.

6.2. Results

Table 3 compares all methods at $\rho = 30\%$ on LLaMA and Mistral. RAP is the only method that simultaneously reduces KV-Cache, model size, and FLOPs while delivering genuine speedup. RAP preserves strong accuracy at $\rho \in [20\%, 30\%]$: PPL and zero-shot accuracy remain near baseline at $\rho = 30\%$, while LongBench is stable at $\rho = 20\%$. At matched KV-Cache compression, RAP achieves the largest reductions in attention parameters/FLOPs and the lowest attention latency among the evaluated methods, while preserving accuracy.

6.2.1. PARAMETER SAVING

RAP simultaneously compresses the KV-Cache and attention parameters with the same ratio, avoiding the parameter overhead inherent in SVD-based factorization (Figure 5, **green** for attention layer and **red** for full model size). At $\rho = 30\%$, RAP reduces attention size to 70.0% of the baseline—perfectly matching the KV-Cache reduction—whereas SVD and PaLU remain at 97.6%-129.5% and 90.7%-111.8% due to the additional matrix introduced by factorization. This linear scaling persists across the 10%-50% range, with detailed results available in Appendix D.7.

6.2.2. FLOPS REDUCTION

RAP also exhibits linear reduction in attention FLOPs with the same factor ρ as KV-Cache. We analytically model KV projection complexity (Table 2), and empirically vali-

Table 3. Comprehensive comparison at $\rho = 30\%$. All metrics relative to no compression baseline (100%). Arrows: \downarrow =better, \uparrow =worse.

Model	Method	KV-Cache Size	Attn Parameters*	Attn FLOPs*	Full Model Parameters*	Latency (Prefill)	Latency (Decode)	PPL
LLaMA	Baseline	100%	100%	100%	100%	100%	100%	8.28
	SVD	70% \downarrow	97.6%-129.5% \uparrow	97.6%-129.5% \uparrow	99.6%-104.9% \uparrow	100.0% \uparrow	196.0% \uparrow	136.50
	PaLU	70% \downarrow	90.7%-111.8% \uparrow	82.5%-111.8% \uparrow	98.5%-102.0% \uparrow	101.0% \uparrow	112.0% \uparrow	9.14
Mistral	Baseline	100%	100%	100%	100%	100%	100%	5.32
	SVD	70% \downarrow	97.6%-129.5% \uparrow	97.6%-129.5% \uparrow	99.6%-104.9% \uparrow	101.0% \uparrow	200.0% \uparrow	42.27
	PaLU	70% \downarrow	90.6%-111.8% \uparrow	82.5%-111.8% \uparrow	98.3%-102.0% \uparrow	100.0% \uparrow	111.0% \uparrow	5.85
	RAP	70% \downarrow	70.0% \downarrow	70.3% \downarrow	95.0% \downarrow	83.0% \downarrow	77.0% \downarrow	8.82

* Ranges reflect factorization granularities: lower bound (per-head, head independently), upper bound (cross-head, all heads jointly), intermediate values from grouped-head factorization. Latency and PPL are measured with per-head factorization.

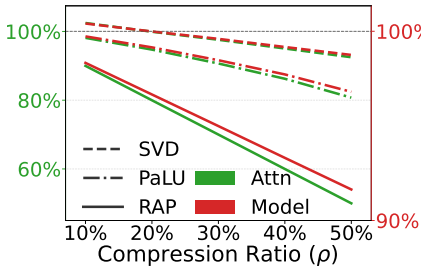


Figure 5. Parameters Relative to Baseline

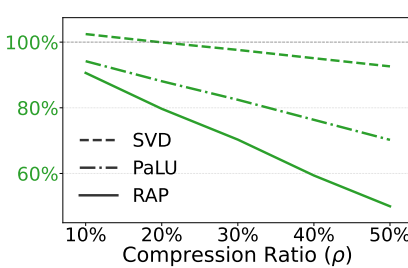


Figure 6. FLOPs Relative to Baseline

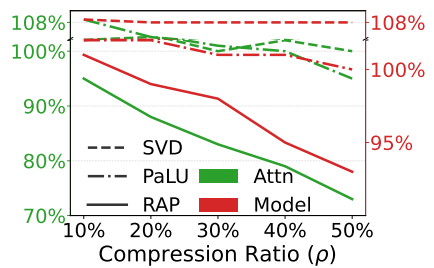


Figure 7. Prefill Latency Relative to Baseline

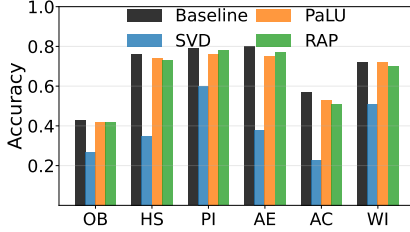
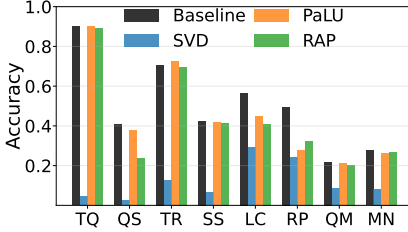
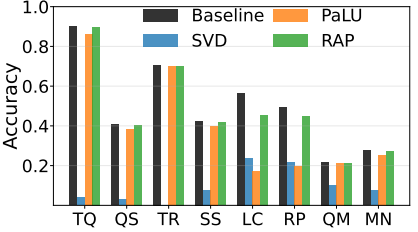

 Figure 8. Zero-shot Accuracy ($\rho = 30\%$)

 Figure 9. LongBench ($\rho = 20\%$)


Figure 10. LongBench (Match Parameters).

Table 4. LLaMA accuracy preservation: PPL (avg. Accuracy).

ρ	Baseline	SVD	PaLU	RAP
10%	8.28(0.68)	30.0(0.47)	8.34(0.67)	8.31(0.67)
20%	8.28(0.68)	74.6(0.41)	8.69(0.66)	8.57(0.67)
30%	8.28(0.68)	136.5(0.39)	9.14(0.65)	8.82(0.65)
40%	8.28(0.68)	366.6(0.37)	9.88(0.62)	9.64(0.63)
50%	8.28(0.68)	1220(0.35)	12.0(0.58)	13.7(0.60)

date the results using ptflops-based measurement (see Appendix D.8), confirming our theoretical predictions. Figure 6 presents the measured results: at $\rho = 30\%$, RAP reduces attention FLOPs by 29.7%—substantially outperforming SVD (2.4%) and PaLU (17.6%).

6.2.3. LATENCY REDUCTION

RAP achieves genuine latency reductions by eliminating reconstruction overhead. We benchmark attention latency and full model E2E latency with sequence length 2k–64k; the

average latency is shown in Figures 7 and 11. At $\rho = 30\%$, RAP reduces attention prefill/decoding latency to 83%/77% of baseline. This advantage grows with ρ : at $\rho = 50\%$, RAP reduces average prefill/decoding latency to 73%/52% of baseline. Full results are in Appendix D.2.

6.2.4. ACCURACY PRESERVATION

We first evaluate WikiText-2 PPL as a general indicator for model accuracy. Table 4 shows that, despite using fewer parameters, RAP achieves comparable PPL as baseline while surpassing PaLU in most cases. We also evaluated each setting on Zero-shot tasks and LongBench, and the results follow the same pattern as PPL.

Zero-shot tasks. We evaluate zero-shot accuracy on six commonsense tasks using lm-eval-harness: OpenBookQA (OB), HellaSwag (HS), PIQA (PI), ARC-Easy (AE), ARC-Challenge (AC), and Winogrande (WI). We report the average accuracy across tasks; Table 4 shows that RAP main-

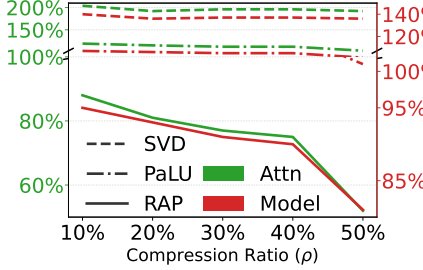


Figure 11. Decode Latency Relative to Baseline

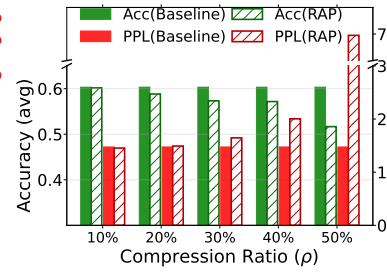
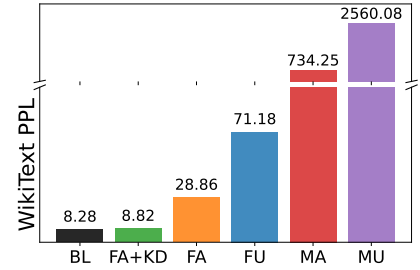
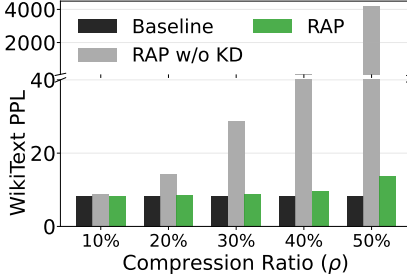

 Figure 12. 4-bit Accuracy ($\rho = 30\%$)

 Figure 13. Strategy Ablation ($\rho = 30\%$)


Figure 14. KD Ablation

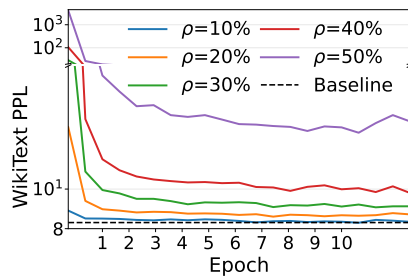


Figure 15. KD PPL Curves

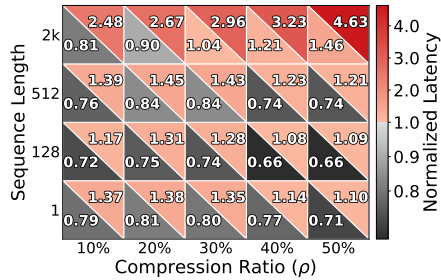


Figure 16. RoPE Latency Relative to Baseline

tains the best average accuracy at $\rho \in [10\%, 40\%]$. Figure 8 shows the per-task behavior at $\rho = 30\%$. Complete results are in Appendix D.6.

LongBench. We evaluate on LongBench with 8 tasks: TriviaQA (TQ), QASPER (QS), TREC (TR), SAMSum (SS), LCC (LC), RepoBench-P (RP), QMSum (QM), and MultiNews (MN). LongBench is more sensitive to parameter reduction than short-context accuracy (Mekala et al., 2025; LI et al., 2025). Despite more aggressive parameter reduction under the same ρ , RAP remains close to baseline until $\rho = 20\%$ (Figure 9). When comparing under the same model parameters, RAP evidently outperforms other methods. For example, matching the parameters of PaLU with $\rho = 30\%$, RAP (47.6%) achieves higher average score than PaLU (39.8%) (Figure 10).

Quantization compatibility. To prove RAP can be combined with *Direct KV-Cache Compression*, we apply 4-bit KV-Cache quantization on top of RAP. Figure 12 reports PPL across ρ ; under 4-bit setting, RAP remains close to baseline. While we cannot test every orthogonal approach, we expect this compatibility to hold for other techniques, including token eviction.

6.3. Ablation Study

Pruning Strategy. We evaluate two key design choices: (i) pair importance scoring (Fisher vs. Magnitude), (ii) rank allocation (adaptive vs. uniform). Figure 13 compares their combinations at $\rho = 30\%$, abbreviated as F (Fisher), M (Magnitude), A (Adaptive), and U (Uniform); FA+KD denotes Fisher+Adaptive with KD, and BL represents Baseline.

Full numbers are reported in Appendix D.9. Results demonstrate that (1) Fisher consistently outperforms Magnitude, (2) Adaptive allocation outperforms Uniform, confirming the effectiveness of each component in RAP.

Knowledge Distillation. Figure 14 demonstrates that KD is essential and effective for accuracy recovery across compression ratios. Figure 15 shows the KD curve for LLaMA, confirming that KD converges quickly and most gains are achieved early during recovery.

Kernel Efficiency. Unlike factorization, RAP only reduces dimensions without modifying the computation graph, guaranteeing speedups. The only potential overhead is non-contiguous RoPE indexing, where PyTorch incurs extra memory copies. We implement non-contiguous RoPE in Triton without memory copies, achieving consistent speedups. Figure 16 shows the comparison at batch size $b = 1$: each cell’s top-right triangle is Triton, bottom-left is PyTorch. Moreover, since RoPE accounts for only $< 1\%$ of inference latency, even using PyTorch, the incurred extra memory copy is still trivial. Full results are in Appendix D.5.

7. Conclusion

We introduce RAP, a structured pruning method that removes RoPE-aligned column pairs under sensitivity-guided budgets. Across the methods we evaluated, RAP uniquely reduces parameters, KV-Cache, and FLOPs without incurring reconstruction overhead, and it combines cleanly with Direct KV-Cache Compression. RAP is a drop-in upgrade for RoPE-based LLMs, requiring no inference-stack changes while preserving accuracy.

Impact Statement

This paper presents work whose goal is to advance the field of machine learning. There are few potential societal consequences of our work, none of which we feel must be specifically highlighted here.

References

Achiam, J., Adler, S., Agarwal, S., Ahmad, L., Akkaya, I., Aleman, F. L., Almeida, D., Altenschmidt, J., Altman, S., Anadkat, S., et al. Gpt-4 technical report. *arXiv preprint arXiv:2303.08774*, 2023.

Bai, J., Bai, S., Chu, Y., Cui, Z., Dang, K., Deng, X., Fan, Y., Ge, W., Han, Y., Huang, F., et al. Qwen technical report. *arXiv preprint arXiv:2309.16609*, 2023.

Beltagy, I., Peters, M. E., and Cohan, A. Longformer: The long-document transformer. *arXiv preprint arXiv:2004.05150*, 2020.

Chang, C.-C., Lin, W.-C., Lin, C.-Y., Chen, C.-Y., Hu, Y.-F., Wang, P.-S., Huang, N.-C., Ceze, L., Abdelfattah, M. S., and Wu, K.-C. Palu: KV-cache compression with low-rank projection. In *The Thirteenth International Conference on Learning Representations*, 2025.

DeepSeek. DeepSeek-V3.2: Mixture-of-experts with 2t active params. <https://huggingface.co/deepseek-ai/DeepSeek-V3.2>, 2025. Model repository.

Eckart, C. and Young, G. The approximation of one matrix by another of lower rank. *Psychometrika*, 1(3):211–218, 1936.

Frantar, E. and Alistarh, D. Sparsegpt: Massive language models can be accurately pruned in one-shot. In *International conference on machine learning*, pp. 10323–10337, 2023.

Frantar, E., Ashkboos, S., Hoefer, T., and Alistarh, D. Gptq: Accurate post-training quantization for generative pre-trained transformers. *arXiv preprint arXiv:2210.17323*, 2022.

Fu, Y. Challenges in deploying long-context transformers: A theoretical peak performance analysis, 2024.

Gholami, A., Yao, Z., Kim, S., Hooper, C., Mahoney, M. W., and Keutzer, K. Ai and memory wall. *IEEE Micro*, 44(3):33–39, 2024.

Hinton, G., Vinyals, O., and Dean, J. Distilling the knowledge in a neural network. *arXiv preprint arXiv:1503.02531*, 2015.

Hooper, C., Kim, S., Mohammadzadeh, H., Mahoney, M. W., Shao, Y. S., Keutzer, K., and Gholami, A. Kvquant: Towards 10 million context length lilm inference with kv cache quantization. *Advances in Neural Information Processing Systems*, 37:1270–1303, 2024.

Hu, E. J., Wallis, P., Allen-Zhu, Z., Li, Y., Wang, S., Wang, L., Chen, W., et al. Lora: Low-rank adaptation of large language models. In *International Conference on Learning Representations*, 2022.

Li, Y., Huang, Y., Yang, B., Venkitesh, B., Locatelli, A., Ye, H., Cai, T., Lewis, P., and Chen, D. Snapkv: Lilm knows what you are looking for before generation. *Advances in Neural Information Processing Systems*, 37:22947–22970, 2024.

LI, Y., Jiang, H., Wu, Q., Luo, X., Ahn, S., Zhang, C., Abdi, A. H., Li, D., Gao, J., Yang, Y., and Qiu, L. SCBench: A KV cache-centric analysis of long-context methods. In *The Thirteenth International Conference on Learning Representations*, 2025. URL <https://openreview.net/forum?id=gkUyYcY1W9>.

Lin, J., Tang, J., Tang, H., Yang, S., Chen, W.-M., Wang, W.-C., Xiao, G., Dang, X., Gan, C., and Han, S. Awq: Activation-aware weight quantization for on-device lilm compression and acceleration. *Proceedings of machine learning and systems*, 6:87–100, 2024.

Lin, Y., Tang, H., Yang, S., Zhang, Z., Xiao, G., Gan, C., and Han, S. Qserve: W4a8kv4 quantization and system co-design for efficient lilm serving. *Proceedings of Machine Learning and Systems*, 7, 2025.

Liu, A., Feng, B., Xue, B., Wang, B., Wu, B., Lu, C., Zhao, C., Deng, C., Zhang, C., Ruan, C., et al. Deepseek-v3 technical report. *arXiv preprint arXiv:2412.19437*, 2024a.

Liu, Z., Yuan, J., Jin, H., Zhong, S., Xu, Z., Braverman, V., Chen, B., and Hu, X. Kivi: a tuning-free asymmetric 2bit quantization for kv cache. In *Proceedings of the 41st International Conference on Machine Learning*, pp. 32332–32344, 2024b.

Lv, B., Zhou, Q., Ding, X., Wang, Y., and Ma, Z. Kvpruner: Structural pruning for faster and memory-efficient large language models. In *ICASSP*, pp. 1–5, 2025. URL <https://doi.org/10.1109/ICASSP49660.2025.10889000>.

Ma, X., Fang, G., and Wang, X. LLM-pruner: On the structural pruning of large language models. In Oh, A., Naumann, T., Globerson, A., Saenko, K., Hardt, M., and Levine, S. (eds.), *Advances in Neural Information Processing Systems*, volume 36, pp. 21702–21720. Curran Associates, Inc., 2023.

Mekala, A., Atmakuru, A., Song, Y., Karpinska, M., and Iyyer, M. Does quantization affect models’ performance on long-context tasks? In Christodoulopoulos, C., Chakraborty, T., Rose, C., and Peng, V. (eds.), *Proceedings of the 2025 Conference on Empirical Methods in Natural Language Processing*, pp. 9422–9470, Suzhou, China, November 2025. Association for Computational Linguistics. ISBN 979-8-89176-332-6. doi: 10.18653/v1/2025.emnlp-main.479. URL <https://aclanthology.org/2025.emnlp-main.479.>

Meta AI. LLaMA-4: Open and efficient foundation language models. <https://huggingface.co/meta-llama/Llama-4-Scout-17B-16E-Instruct>, 2025. Model repository.

Mistral. Mistral Small 3.2. <https://huggingface.co/mistralai/Mistral-Small-3.2-24B-Instruct-2506>, 2025. Model repository.

OpenAI. GPT-OSS: Open source generative pre-trained transformer. <https://huggingface.co/openai/gpt-oss-20b>, 2025. Model repository.

Peng, B., Quesnelle, J., Fan, H., and Shippole, E. Yarn: Efficient context window extension of large language models. URL <https://arxiv.org/abs/2309.00071>, 2023.

Qwen. Qwen-3-Next: A next-generation vision-language model. <https://huggingface.co/Qwen/Qwen3-Next-80B-A3B-Instruct>, 2025. Model repository.

Sun, M., Liu, Z., Bair, A., and Kolter, J. Z. A simple and effective pruning approach for large language models. In *The Twelfth International Conference on Learning Representations*, 2024.

Touvron, H., Lavril, T., Izacard, G., Martinet, X., Lachaux, M.-A., Lacroix, T., Rozière, B., Goyal, N., Hambro, E., Azhar, F., et al. Llama: Open and efficient foundation language models. *arXiv preprint arXiv:2302.13971*, 2023.

Vaswani, A., Shazeer, N., Parmar, N., Uszkoreit, J., Jones, L., Gomez, A. N., Kaiser, Ł., and Polosukhin, I. Attention is all you need. *Advances in neural information processing systems*, 30, 2017.

Wang, C., Guo, J., Li, H., Tian, Y., Nie, Y., Xu, C., and Han, K. Circle-rope: Cone-like decoupled rotary positional embedding for large vision-language models. *arXiv preprint arXiv:2505.16416*, 2025a.

Wang, X., Zheng, Y., Wan, Z., and Zhang, M. SVD-LLM: Truncation-aware singular value decomposition for large language model compression. In *The Thirteenth International Conference on Learning Representations*, 2025b.

Zaheer, M., Guruganesh, G., Dubey, K. A., Ainslie, J., Alberti, C., Ontanon, S., Pham, P., Ravula, A., Wang, Q., Yang, L., et al. Big bird: Transformers for longer sequences. *Advances in neural information processing systems*, 33:17283–17297, 2020.

Zhang, Z., Sheng, Y., Zhou, T., Chen, T., Zheng, L., Cai, R., Song, Z., Tian, Y., Ré, C., Barrett, C., et al. H2o: Heavy-hitter oracle for efficient generative inference of large language models. *Advances in Neural Information Processing Systems*, 36:34661–34710, 2023.

Zhipu AI. GLM-4.7: Scaling logic and reasoning. <https://huggingface.co/zai-org/GLM-4.7>, 2026. Model repository.

A. LLM Assistance Statement.

We only used LLM as a writing assistant to improve grammar and presentation clarity. All scientific claims were produced and verified by the authors; the LLM did not generate or modify any experimental data.

B. Error Bound Derivation

We provide the complete derivation for the loss bound stated in Section 5.

B.1. Proof of Theorem 5.1

Proof. Let $\Delta W_k = A_k - W_k$ denote the pruning-induced perturbation to the key projection matrix. Since RAP removes entire RoPE pairs, ΔW_k is block-sparse with respect to the RoPE pair decomposition, with nonzero entries only on the pruned pairs $p \notin \mathcal{S}$.

Assuming \mathcal{L} is twice continuously differentiable with respect to W_k , a second-order Taylor expansion around W_k yields

$$\Delta \mathcal{L} = \frac{1}{2} \langle \Delta W_k, \nabla_{W_k}^2 \mathcal{L} \Delta W_k \rangle. \quad (15)$$

We approximate the Hessian $\nabla_{W_k}^2 \mathcal{L}$ using the Fisher information matrix, which is standard in second-order pruning analyses (Frantar & Alistarh, 2023).

Moreover, because RoPE applies independent 2×2 orthogonal rotations to each feature pair, cross-pair interactions are negligible, and the Fisher matrix can be approximated as block-diagonal over RoPE pairs. Under this approximation, the quadratic form decomposes additively:

$$\Delta \mathcal{L} \leq \frac{1}{2} \sum_{p \notin \mathcal{S}} \langle \Delta W_k^{(p)}, \mathbf{F}^{(p)} \Delta W_k^{(p)} \rangle = \frac{1}{2} \sum_{p \notin \mathcal{S}} \sigma_p, \quad (16)$$

where $\Delta W_k^{(p)}$ denotes the restriction of ΔW_k to RoPE pair p and σ_p is the aggregated Fisher score defined in Eq. (7). This completes the proof. \square

C. Derivation for Table 2

Table 2 reports symbol-level scaling for KV-Cache size, parameters, and FLOPs for **computing the KV-Cache** for a **single K/V head** with the full input dimension $\hat{D}=HD$ (so each projection matrix is $\hat{D} \times D$). We only count \mathbf{W}_k and \mathbf{W}_v and the runtime work needed to produce the cached K/V states. In particular, the FLOPs entries for SVD/PaLU include reconstruction: SVD reconstructs both K and V, while PaLU reconstructs only K (V is absorbed into \mathbf{W}_o). Notation: sequence length S , per-head output dimension D , number of heads H , and retained ratio $r=1-\rho$.

C.1. Baseline.

\mathbf{W}_k and \mathbf{W}_v are each $\hat{D} \times D = HD \times D$. Computing and storing full \mathbf{K} , \mathbf{V} yields KV-Cache $2SD$; parameters for K and V together are $2HD^2$; per-token FLOPs for the two projections are $4SHD^2$. This is the first row of Table 2.

C.2. SVD.

For each of \mathbf{W}_k and \mathbf{W}_v , factorize $\mathbf{W} \approx \mathbf{AB}$ with rank rD , where $\mathbf{A} \in \mathbb{R}^{\hat{D} \times rD}$ and $\mathbf{B} \in \mathbb{R}^{rD \times D}$.

KV-Cache: we store latent $\mathbf{K}_{\text{lat}} = \mathbf{XA}_k \in \mathbb{R}^{S \times rD}$ and $\mathbf{V}_{\text{lat}} = \mathbf{XA}_v \in \mathbb{R}^{S \times rD}$, so KV-Cache scales by r . **Parameters:** the two \mathbf{A} matrices contribute $2\hat{D} \cdot rD = 2rHD^2$ parameters, and the two reconstruction matrices contribute $2(rD) \cdot D = 2rD^2$ parameters, yielding

$$\begin{aligned} \text{Paramssvd} &= 2rHD^2 + 2rD^2 \\ &= 2HD^2 \left(r + \frac{r}{H} \right) \\ &= \left(r + \frac{r}{H} \right) \cdot (2HD^2). \end{aligned} \quad (17)$$

FLOPs: to compute the cached states, we (i) project to latent, costing $2S\hat{D} \cdot rD$ for each of K and V, and (ii) reconstruct full-dimensional K and V via $(\mathbf{XA})\mathbf{B}$, costing $2S(rD) \cdot D$ for each. Thus

$$\begin{aligned} \text{Flopssvd} &= 4S\hat{D}rD + 4S(rD)D \\ &= 4SHD^2 \left(r + \frac{r}{H} \right) \\ &= \left(r + \frac{r}{H} \right) \cdot (4SHD^2). \end{aligned} \quad (18)$$

C.3. PaLU.

PaLU applies data whitening and absorbs the V-side reconstruction into \mathbf{W}_o , so V is stored as latent without reconstructing to D during KV-Cache computation, while K still requires reconstruction.

KV-Cache: KV-Cache still scales by r (store \mathbf{XA}_k and \mathbf{XA}_v).

Parameters: K uses $(\mathbf{A}_k, \mathbf{B}_k)$ while V uses only \mathbf{A}_v (since \mathbf{B}_v is absorbed), so

$$\begin{aligned} \text{Params}_{\text{Palu}} &= \underbrace{\hat{D} \cdot rD + rD \cdot D}_{K} + \underbrace{\hat{D} \cdot rD}_{V} \\ &= 2rHD^2 + rD^2 \\ &= \left(r + \frac{r}{2H} \right) \cdot (2HD^2). \end{aligned} \quad (19)$$

FLOPs: K computes \mathbf{XA}_k and reconstructs $(\mathbf{XA}_k)\mathbf{B}_k$,

while V computes only $\mathbf{X}\mathbf{A}_v$. Therefore

$$\begin{aligned} \text{FLOPs}_{\text{PaLU}} &= \underbrace{\left(2S\hat{D}rD + 2S(rD)D\right)}_K + \underbrace{\left(2S\hat{D}rD\right)}_V \\ &= 4SHD^2 \left(r + \frac{r}{2H}\right) \\ &= \left(r + \frac{r}{2H}\right) \cdot (4SHD^2). \end{aligned} \quad (20)$$

C.4. RAP.

RAP prunes whole RoPE pairs, so the retained columns form $\mathbf{A}_k, \mathbf{A}_v \in \mathbb{R}^{\hat{D} \times rD}$. The expansion is a binary index map that can be absorbed, so KV-Cache computation uses only the low-dimensional projections without reconstruction:

$$\begin{aligned} \text{KVCache}_{\text{RAP}} &= 2S(rD) = r \cdot (2SD), \\ \text{Params}_{\text{RAP}} &= 2\hat{D} \cdot rD = r \cdot (2HD^2), \\ \text{FLOPs}_{\text{RAP}} &= 4S\hat{D} \cdot rD = r \cdot (4SHD^2), \end{aligned} \quad (21)$$

matching the linear- r row in Table 2.

Scope. These derivations isolate the KV-projection ($\mathbf{W}_k, \mathbf{W}_v$) cost for one head with input dimension $\hat{D} = HD$. The empirical tables later in the appendix evaluate practical architectures and full attention blocks (e.g., GQA, RoPE, and different factorization granularities), where the absorption/reconstruction patterns and the accounting (attention-only vs. full-model) can differ from Table 2.

D. Complete Experimental Results

This appendix provides complete tables and supplementary plots for all experiments. Compression ratios are reported as 10%–50% (retain 0.9–0.5). Unless stated otherwise, results are for the same settings as the main text.

D.1. Mistral Figures

This section presents Mistral-specific experimental results. Figures 17, 18, 19, 20, 21, and 22 show memory compression, FLOPs, latency, accuracy, quantization, and ablation results for Mistral-7B-v0.3, complementing the LLaMA results in the main text.

D.2. Complete Latency Tables

Tables 16 and 17 provide the full latency measurements for attention-only and full-model latency, respectively. These measurements correspond to Figures 7 and 11 in the main text. Figure 25 plots the corresponding attention-layer speedup curves across compression ratios for LLaMA and Mistral.

Discussion on PaLU’s original implementation. PaLU’s paper reports a 189% speedup, which primarily stems from a custom fused kernel that combines Q/K/V/O projections, low-rank K/V reconstruction, RoPE, and attention computation (Chang et al., 2025). For fair comparison, we implement an equivalent fused kernel and evaluate RAP under the same setting that PaLU uses; we report the optimized-vs-optimized comparison; RAP remains about 34% faster than PaLU in decoding at $\rho = 50\%$, demonstrating that RAP’s speedup advantage persists even when both methods use optimized kernel implementations.

D.3. PaLU+KD

We attempted to apply the same KD/LoRA recovery recipe to PaLU for a compute-matched comparison. In our preliminary trials, the gains were marginal and sensitive to the loss design; therefore we do not include PaLU+KD curves in the main plots. Table 7 summarizes the WikiText-2 PPL comparison at $\rho = 30\%$.

D.4. Reproducibility

Table 15 summarizes the key hyperparameters and random seeds used in our experiments.

Variance and sensitivity. (i) **Runtime variance.** Latency results are obtained via CUDA-event timing with warmup and multiple repeats; we report avg% (max%) across the tested sequence-length range to mitigate run-to-run noise. (ii) **Seed stability.** Unless otherwise noted, we use fixed seeds for pruning, evaluation, and finetuning; in our experience the qualitative trends (method ranking and ρ -sweeps) are stable across reasonable reruns. (iii) **Hyperparameter / calibration sensitivity.** Fisher estimation uses a small calibration set; we do not observe material changes in selected RoPE pairs or downstream accuracy trends under reasonable variations of calibration size/dataset and KD settings around our defaults (e.g., varying N , substituting C4, or adjusting KD temperature/weights).

D.5. RoPE Kernel Microbenchmark

We benchmark RoPE application on A100-80GB (bfloat16) with $n_{\text{heads}} = 32$, $d_{\text{head}} = 128$, batches $b \in \{1, 2, 4\}$, and sequence lengths $S \in \{1, 128, 512, 2048\}$. We compare the contiguous baseline against PyTorch non-contiguous indexing and our fused Triton kernel. Table 8 reports the baseline latency, and Table 11 reports speedup relative to that baseline (Torch/Triton).

D.6. Complete Accuracy Tables

We report WikiText-2 PPL and zero-shot accuracy on six commonsense tasks (OBQA, HS, PIQA, ARCE, ARCC, Wino). Table 9 highlights the $\rho = 30\%$ case for LLaMA,

while Tables 13 and 14 provide the full results for all compression ratios and both models. Unless noted otherwise, RAP denotes the KD/LoRA recovery used in our main experiments.

D.7. Complete Memory Compression Tables

Table 10 contains full KV-Cache, attention, and total-model ratios. Figure 24 highlights the attention parameter ratios that drive Figure 5 in the main text.

D.8. Complete FLOPs Tables

Table 6 reports KV-projection-only FLOPs implied by Table 2. Table 12 lists measured matmul-only FLOPs for the full attention block. Note that LLaMA and Mistral have identical FLOPs values, as both models share the same attention architecture. Figure 23 visualizes the same attention-block measurements for both models, corresponding to Figure 6 in the main text.

D.9. KD Ablation

Table 5 lists the post-finetuning PPL values in Figure 14.

Table 5. KD ablation across compression ratios (WikiText-2 PPL, LLaMA).

Compression	Baseline	RAP (w/o KD)	RAP
10%	8.28	8.85	8.31
20%	8.28	14.19	8.57
30%	8.28	28.86	8.82
40%	8.28	105.74	9.64
50%	8.28	4189.06	13.74

Table 6. KV-projection-only per-head per-token FLOPs implied by Table 2 (one head; $H=32$, $D=128$; mul+add counts as 2 FLOPs). Baseline is 2.097M.

Ratio	SVD		PaLU		RAP	
	FLOPs (M)	Saving	FLOPs (M)	Saving	FLOPs (M)	Saving
10%	1.946	7.2%	1.917	8.6%	1.887	10.0%
20%	1.730	17.5%	1.704	18.8%	1.678	20.0%
30%	1.514	27.8%	1.491	28.9%	1.468	30.0%
40%	1.298	38.1%	1.278	39.1%	1.258	40.0%
50%	1.081	48.4%	1.065	49.2%	1.049	50.0%

Table 7. WikiText-2 PPL at $\rho = 30\%$: baseline vs. PaLU/RAP with and without KD/LoRA.

Method	LLaMA PPL		Mistral PPL	
	w/o KD	+KD	w/o KD	+KD
Baseline	8.28	8.28	5.32	5.32
PaLU	9.14	8.80	5.85	5.70
RAP	28.86	8.82	26.77	5.68

Table 8. Contiguous RoPE baseline latency (ms).

Batch	S=1	S=128	S=512	S=2048
1	0.105	0.099	0.113	0.394
2	0.099	0.098	0.189	0.758
4	0.103	0.112	0.393	1.457

Table 9. Zero-shot accuracy (LLaMA) at $\rho = 30\%$.

Method	PPL	OBQA	HS	PIQA	ARCE	ARCC	Wino
Baseline	8.28	0.43	0.76	0.79	0.80	0.57	0.72
PaLU	9.14	0.42	0.74	0.76	0.75	0.53	0.72
RAP	8.82	0.42	0.74	0.78	0.77	0.51	0.70

Table 10. Memory compression ratios relative to baseline (100%). Note that **KV-Cache** reduction is identical across all methods. Values $> 100\%$ indicate parameter overhead. **Bold** indicates the best compression (lowest percentage).

Model	Ratio	KV-Cache	Attention Size (%)			Full Model (%)		
			SVD	PaLU	RAP	SVD	PaLU	RAP
LLaMA	10%	90%	102.46	98.13	89.99	100.41	99.73	98.33
	20%	80%	99.92	94.72	79.98	99.99	99.15	96.66
	30%	70%	97.58	90.68	70.00	99.60	98.47	94.99
	40%	60%	95.04	86.24	59.99	99.17	97.72	93.31
	50%	50%	92.50	80.75	50.00	98.75	96.80	91.64
Mistral	10%	90%	102.46	98.01	89.99	100.46	99.68	98.15
	20%	80%	99.92	94.50	79.98	99.99	99.02	96.29
	30%	70%	97.58	90.63	70.00	99.55	98.29	94.44
	40%	60%	95.04	85.18	59.99	99.08	97.28	92.59
	50%	50%	92.50	79.74	50.00	98.61	96.26	90.74

Table 11. Torch/Triton speedup vs. contiguous baseline. Values are $\text{Speedup}_{\text{Torch}} / \text{Speedup}_{\text{Triton}}$.

Comp.	b=1		b=2		b=4	
	S=512	S=2048	S=512	S=2048	S=512	S=2048
50%	0.74 / 1.21	1.46 / 4.63	1.23 / 2.12	1.54 / 7.55	1.70 / 4.34	1.68 / 7.75
40%	0.74 / 1.23	1.21 / 3.23	1.14 / 2.07	1.30 / 3.11	1.45 / 3.27	1.38 / 3.14
30%	0.84 / 1.43	1.04 / 2.96	1.03 / 2.39	1.13 / 2.84	1.24 / 3.08	1.19 / 2.91
20%	0.84 / 1.45	0.90 / 2.67	0.93 / 2.17	0.99 / 2.61	1.05 / 2.75	1.04 / 2.64
10%	0.76 / 1.39	0.81 / 2.48	0.84 / 2.11	0.89 / 2.50	0.94 / 2.57	0.93 / 2.51

Table 12. Measured attention-block per-head per-token FLOPs and relative savings compared to the Baseline (2.654M). **Bold** indicates the best method (lowest FLOPs / highest saving).

Model	Ratio	FLOPs (M)			Saving vs Baseline		
		SVD	PaLU	RAP	SVD	PaLU	RAP
LLaMA	10%	2.719	2.500	2.405	-2.4%	5.8%	9.4%
	20%	2.652	2.338	2.115	0.1%	11.9%	20.3%
	30%	2.591	2.188	1.866	2.4%	17.6%	29.7%
	40%	2.524	2.026	1.576	4.9%	23.6%	40.6%
	50%	2.458	1.864	1.327	7.4%	29.8%	50.0%
Mistral	10%	2.719	2.500	2.405	-2.4%	5.8%	9.4%
	20%	2.652	2.338	2.115	0.1%	11.9%	20.3%
	30%	2.591	2.188	1.866	2.4%	17.6%	29.7%
	40%	2.524	2.026	1.576	4.9%	23.6%	40.6%
	50%	2.458	1.864	1.327	7.4%	29.8%	50.0%

Table 13. LLaMA zero-shot accuracy results. We report PPL and accuracy metrics (OBQA, HellaSwag, PIQA, ARC-Easy, ARC-Challenge, WinoGrande) across compression ratios from 10% to 50%.

Ratio	Method	PPL	OBQA	HS	PIQA	ARCE	ARCC	Wino
10%	Baseline	8.28	0.43	0.76	0.79	0.80	0.57	0.72
	SVD	30.00	0.32	0.52	0.65	0.43	0.28	0.59
	PaLU	8.34	0.43	0.76	0.77	0.79	0.57	0.72
	RAP	8.31	0.43	0.75	0.79	0.79	0.57	0.71
20%	Baseline	8.28	0.43	0.76	0.79	0.80	0.57	0.72
	SVD	74.64	0.29	0.40	0.61	0.39	0.26	0.53
	PaLU	8.69	0.42	0.75	0.77	0.76	0.53	0.72
	RAP	8.57	0.44	0.75	0.78	0.78	0.55	0.70
30%	Baseline	8.28	0.43	0.76	0.79	0.80	0.57	0.72
	SVD	136.50	0.27	0.35	0.60	0.38	0.23	0.51
	PaLU	9.14	0.42	0.74	0.76	0.75	0.53	0.72
	RAP	8.82	0.42	0.73	0.78	0.77	0.51	0.70
40%	Baseline	8.28	0.43	0.76	0.79	0.80	0.57	0.72
	SVD	366.60	0.25	0.31	0.56	0.34	0.23	0.54
	PaLU	9.88	0.42	0.70	0.75	0.70	0.47	0.68
	RAP	9.64	0.43	0.71	0.77	0.73	0.48	0.68
50%	Baseline	8.28	0.43	0.76	0.79	0.80	0.57	0.72
	SVD	1220.27	0.25	0.29	0.54	0.32	0.23	0.50
	PaLU	12.03	0.39	0.62	0.74	0.66	0.42	0.64
	RAP	13.74	0.41	0.68	0.75	0.68	0.42	0.64

Table 14. Mistral zero-shot accuracy results. We report PPL and accuracy metrics (OBQA, HellaSwag, PIQA, ARC-Easy, ARC-Challenge, WinoGrande) across compression ratios from 10% to 50%.

Ratio	Method	PPL	OBQA	HS	PIQA	ARCE	ARCC	Wino
10%	Baseline	5.32	0.44	0.80	0.82	0.78	0.52	0.74
	SVD	10.41	0.36	0.57	0.74	0.51	0.30	0.61
	PaLU	5.40	0.45	0.80	0.82	0.78	0.52	0.71
	RAP	5.34	0.45	0.80	0.82	0.78	0.52	0.73
20%	Baseline	5.32	0.44	0.80	0.82	0.78	0.52	0.74
	SVD	21.26	0.29	0.49	0.67	0.40	0.25	0.53
	PaLU	5.56	0.43	0.80	0.81	0.76	0.51	0.70
	RAP	5.52	0.44	0.79	0.81	0.78	0.52	0.72
30%	Baseline	5.32	0.44	0.80	0.82	0.78	0.52	0.74
	SVD	42.27	0.29	0.44	0.64	0.37	0.24	0.54
	PaLU	5.85	0.43	0.78	0.80	0.75	0.48	0.70
	RAP	5.85	0.43	0.78	0.81	0.76	0.48	0.70
40%	Baseline	5.32	0.44	0.80	0.82	0.78	0.52	0.74
	SVD	77.72	0.25	0.37	0.59	0.34	0.24	0.52
	PaLU	5.98	0.43	0.74	0.79	0.72	0.44	0.69
	RAP	6.40	0.44	0.76	0.79	0.73	0.45	0.67
50%	Baseline	5.32	0.44	0.80	0.82	0.78	0.52	0.74
	SVD	138.63	0.26	0.31	0.56	0.32	0.23	0.51
	PaLU	6.43	0.41	0.70	0.78	0.68	0.40	0.67
	RAP	10.94	0.42	0.72	0.77	0.69	0.40	0.62

Table 15. Reproducibility checklist: key experimental settings and random seeds.

Component	Key settings (defaults)
Pruning	Per-head pruning by default; export dtype <code>bfloat16</code> . RAP scoring uses <code>wikitext-2-raw-v1</code> , <code>importance-batches=4</code> , <code>importance-batch-size=4</code> , <code>importance-seq-len=2048</code> ; full-model Fisher uses <code>fisher-samples=32</code> and <code>fisher-seq-len=2048</code> . Seed: 42.
Attention-layer latency (prefill)	CUDA event timing; backend <code>eager</code> or <code>sdpa</code> ; dtype <code>float16</code> ; batch list default <code>{1}</code> ; seq list default 2k–64k; warmup 5, repeat 20; RAP optionally enables Triton RoPE via <code>--triton</code> . Seed: 42.
Attention-layer latency (decoding)	CUDA event timing; backend <code>eager</code> or <code>sdpa</code> ; dtype <code>float16</code> ; batch list default <code>{1}</code> ; KV lengths 2k–64k; warmup 10, repeat 100; prime warmup <code>prime-kv=4096</code> and <code>prime-steps=3</code> ; optional random KV-Cache via <code>--random-cache</code> . Seed: 42.
Accuracy (PPL + lm-eval)	PPL on WikiText-2 with <code>seqlen=2048</code> and <code>batch-size=8</code> ; zero-shot tasks: OpenBookQA, HellaSwag, PIQA, ARC-Easy, ARC-Challenge, WinoGrande. Seed: 42.
LongBench	Greedy decoding (<code>do_sample=False</code> , <code>num_beams=1</code>); KV-Cache enabled when supported. Seed: 42.
KD + LoRA finetuning	Global batch 128, micro-batch 8, epochs 20, lr 10^{-4} , cutoff-len 256; LoRA $r_{\text{LoRA}}=8$, $\alpha=16$, dropout 0.05; KD weights $\alpha_{\text{CE}}=0.4$, $\alpha_{\text{KD}}=0.6$, temperature $T=2.0$. Seed: 42.

Table 16. Attention layer latency speedup (avg%(max%)) vs baseline.

Model	Ratio	Prefill			Decoding		
		SVD	PaLU	RAP	SVD	PaLU	RAP
LLaMA	10%	98%(103%)	92%(103%)	105%(118%)	49%(66%)	84%(96%)	114%(132%)
	20%	97%(103%)	97%(106%)	114%(154%)	52%(68%)	87%(99%)	123%(145%)
	30%	100%(105%)	99%(110%)	120%(164%)	51%(66%)	89%(96%)	130%(139%)
	40%	98%(105%)	100%(114%)	127%(179%)	51%(64%)	89%(93%)	133%(141%)
	50%	100%(108%)	105%(123%)	137%(196%)	52%(65%)	97%(102%)	192%(303%)
Mistral	10%	95%(101%)	93%(100%)	105%(118%)	49%(65%)	84%(97%)	115%(133%)
	20%	98%(102%)	97%(106%)	116%(154%)	51%(65%)	84%(95%)	123%(128%)
	30%	99%(108%)	100%(110%)	120%(164%)	50%(67%)	90%(97%)	132%(141%)
	40%	99%(108%)	102%(127%)	127%(179%)	51%(65%)	91%(101%)	132%(143%)
	50%	101%(108%)	106%(123%)	139%(200%)	53%(66%)	96%(101%)	192%(303%)

Table 17. Full model latency speedup (avg%(max%)) vs baseline.

Model	Ratio	Prefilling			Decoding		
		SVD	PaLU	RAP	SVD	PaLU	RAP
LLaMA	10%	92%(96%)	98%(99%)	99%(102%)	71%(83%)	93%(98%)	105%(110%)
	20%	93%(96%)	98%(100%)	101%(105%)	74%(85%)	94%(100%)	108%(114%)
	30%	93%(97%)	99%(101%)	102%(108%)	73%(83%)	96%(98%)	110%(112%)
	40%	93%(97%)	99%(102%)	105%(111%)	73%(82%)	96%(97%)	111%(113%)
	50%	93%(97%)	100%(103%)	108%(115%)	74%(83%)	99%(101%)	123%(135%)
Mistral	10%	92%(96%)	97%(100%)	99%(103%)	71%(83%)	93%(99%)	105%(111%)
	20%	92%(97%)	98%(101%)	101%(106%)	73%(83%)	93%(98%)	108%(109%)
	30%	93%(97%)	99%(102%)	102%(108%)	72%(84%)	96%(99%)	110%(113%)
	40%	93%(98%)	99%(103%)	105%(112%)	73%(83%)	96%(100%)	110%(113%)
	50%	93%(98%)	100%(106%)	108%(114%)	74%(83%)	98%(100%)	123%(135%)

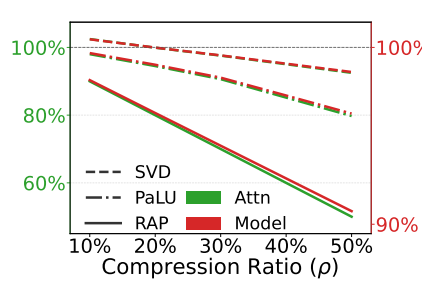


Figure 17. Parameters Relative to Baseline (Mistral)

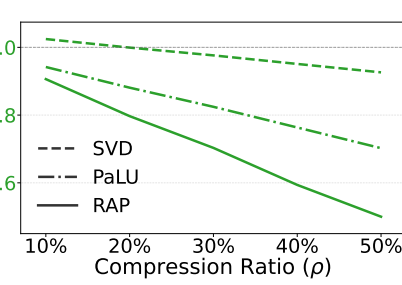


Figure 18. FLOPs Relative to Baseline (Mistral)

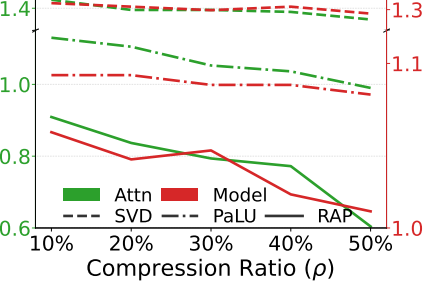


Figure 19. Prefill Latency Relative to Baseline (Mistral)

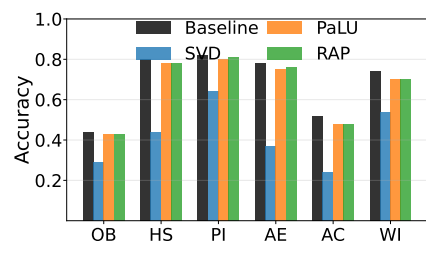


Figure 20. Zero-shot Accuracy ($\rho = 30\%$) (Mistral)

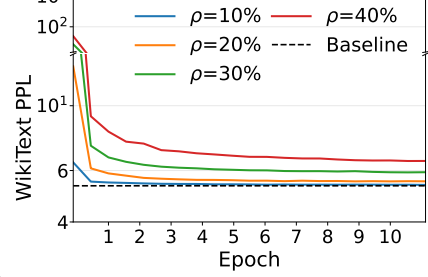


Figure 21. KD PPL Curves (Mistral)

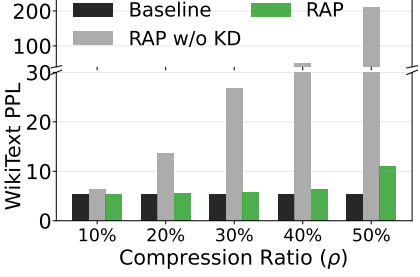


Figure 22. KD Ablation (Mistral)

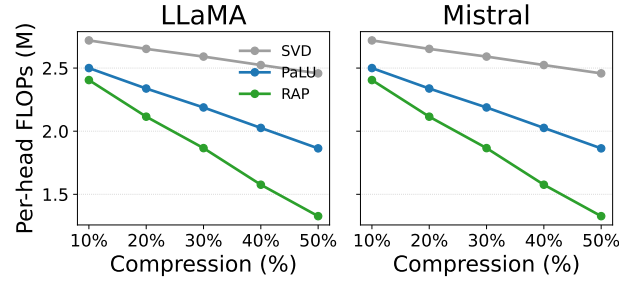


Figure 23. Measured per-head per-token FLOPs vs. compression ratio for LLaMA and Mistral.

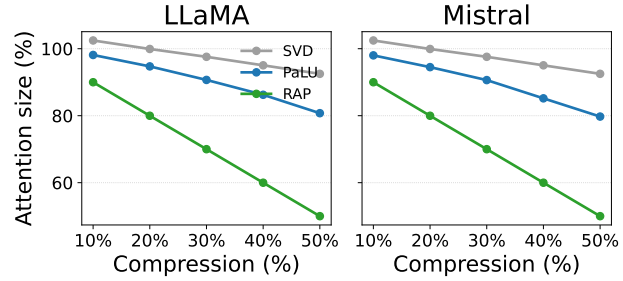


Figure 24. Attention parameter size vs. compression ratio for LLaMA and Mistral.

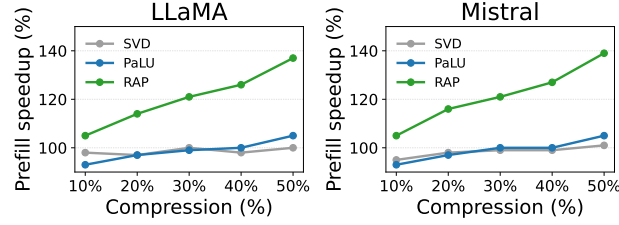


Figure 25. Latency speedup vs. compression ratio for LLaMA and Mistral. We plot attention-layer speedup (prefill/decode) across compression ratios; full-model values are listed in Table 17.